ACS APPLIED MATERIALS & INTERFACES

Research Article

www.acsami.org

Differential Cell Adhesion on Mesoporous Silicon Substrates

Francesco Gentile,[†,‡] Rosanna La Rocca,[‡] Giovanni Marinaro,[‡] Annalisa Nicastri,[†] Andrea Toma,[‡] Francesco Paonessa,[‡] Gheorghe Cojoc,[§] Carlo Liberale,[‡] Fabio Benfenati,[‡] Enzo di Fabrizio,[†,‡] and Paolo Decuzzi*[,†,⊥]

[†]Laboratory of Proteomics and Mass Spectrometry, Department of Experimental and Clinical Medicine, University of Magna Graecia, Catanzaro 88100, Italy

[‡]Italian Institute of Technology Nanostructure and NBT Departments, Via Morego, 30, 16163 Genova, Italy

[§]Max Planck Institute of Molecular Cell Biology and Genetics, Pfotenhauerstrasse 108, 01307 Dresden, Germany

[⊥]Departments of Translational Imaging & Nanomedicine, The Methodist Hospital Research Institute, Houston, Texas 77030, United States

Supporting Information

ABSTRACT: Porous silicon (PSi) is a promising material in several biomedical applications because of its biocompatibility and biodegradability. Despite the plethora of studies focusing on the interaction of cells with micrometer and submicro geometrical features, limited information is available on the response of cells to substrates with a quasi-regular distribution of nanoscopic pores. Here, the behavior of four different cell types is analyzed on two mesoporous (MeP) silicon substrates, with an average pore size of ∼5 (MeP1) and ∼20 nm (MeP2), respectively. On both MeP substrates, cells are observed to spread and adhere in a larger number as compared to flat silicon wafers. At all considered time points, the surface density of the adhering cells n_d is larger on the PSi substrate with the smaller average pore size (MeP1). At 60 h, n_d is from ∼1.5 to 5 times larger on MeP1 than on MeP2 substrates, depending on the cell type. The higher rates of proliferation are observed for the two neuronal cell types, the mouse neuroblastoma cells (N2A) and the immortalized human cortical neuronal cells (HCN1A). It is speculated that the higher adhesion on MeP1 could be attributed to a preferential matching of the substrate topography with the recently observed multiscale molecular architecture of focal adhesions. These results have implications in the rational development of PSi substrates for supporting cell adhesion and controlling drug release in implants and scaffolds for tissue engineering applications.

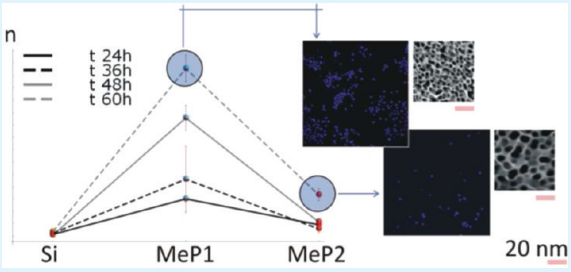

KEYWORDS: *mesoporous silicon, nanoscale topography, cell adhesion, optimal pore size, silicon implants, tissue engineering*

1. INTRODUCTION

The growing interest in porous silicon (PSi) for several biomedical applications is justified by its distinctive advantages over other more traditional materials, such as polymers. PSi can be produced using top-down and quite inexpensive fabrication strategies.[1] In addition, robust protocols are available for its surface modification with a variety of functional groups and biomolecules.[2,3] Also, the pore size, pitch, and shape (pore geometry) can be accurately tuned, during the fabrication process, by judiciously choosing parameters such as the etching time, current intensity, active etchant concentration, temperature and silicon doping.[1] According to the IUPAC definition, surfaces with a pore size smaller than 2 nm are referred to as microporous; whereas mesoporous PSi (MeP) exhibits pores with an average size ranging between 2 and 50 nm; and, eventually, for pores larger than 50 nm, the term macroporous PSi (MaP) is used. Differently from bulk silicon, PSi is biodegradable under physiological conditions and it dissolves progressively into nontoxic silicic acid. The dissolution rate is dependent on the pore geometry and surface modification, and it grows as the pore size increases.[4] Several studies have demonstrated the biocompatibility of PSi under different conditions.[5−8] In addition to this, PSi offers very interesting photoluminescence properties which are dependent on pore geometry and disappear for pores larger than a few tens of nanometers.[9,10]

For all this, PSi has been proposed and is currently used for the fabrication of diverse micro- and nanodevices of interest to the biomedical community. Microchips made out of PSi for the controlled release of drugs were already demonstrated in the '90s,[11] and thereafter by several researchers.[12,13] With the advent of more sophisticated miniaturization techniques, PSi nanoparticles have been fabricated and used for the systemic administration of therapeutic and imaging agents.[14−16] Because of its inherent optical properties, biosensors and bio-optoelectronic devices are also generated out of PSi.[17] MiP

Received: January 16, 2012
Accepted: May 14, 2012
Published: May 14, 2012

and MeP substrates have been shown to be extremely promising in developing new plasma fractionation techniques for proteomic analysis.[18,19] PSi-based scaffolds for orthopedic implants[20] and for controlling the adhesion and proliferation of different cell types, including neurons[21] and hepatocytes,[22] have been proposed too. Eye implants for the controlled and long-term release of drugs within the ocular bulb have also been reported.[23]

Substrate topography has been known for a long time to affect crucial cell functions, such as adhesion, proliferation, migration and differentiation.[24] This has been extensively characterized on different materials and on substrates exhibiting diverse topographical features, such as pits, holes, ridges, at the micrometer and submicrometer scale (>100 nm).[25−29] Despite all this, most of the studies on PSi have focused on the effect of surface chemistries on cell adhesion and proliferation.[21,22,30,31] Recently, a hand-full of manuscripts have started interrogating on how pore geometry could affect the cellular response. In Sapelkin et al., rat hippocampal neurons were observed to preferentially adhere on MaP surfaces, with a pore size ranging between 50 and 100 nm, rather than on flat silicon surfaces.[32] A broader range of pore sizes was considered in Khung et al., where neuroblastoma cells (SK-N-SH) were cultured over continuous porous gradient substrates spanning across the MeP and MaP regimes.[33] It was shown that substrates with an average pore sizes in the few hundreds of nanometers restrict cell proliferation and adhesion within the first 24 h. This was confirmed in a more recent study, with osteoblasts, cultured over substrates with pore sizes of 100, 300, and 500 nm.[34]

In this manuscript, the adhesive behavior of four distinct cell types is analyzed up to 60 h post seeding on oxidized PSi substrates presenting a pore size ranging between ∼5 and 20 nm. This indeed is the more relevant pore size for biomedical applications pertaining to the in vivo controlled delivery of drugs from PSi implants and the in vitro harvesting of low molecular weight proteins from plasma. The four cell types are mouse 3T3 fibroblasts and human vascular endothelial cells (HUVECs), often used as reference cells in biocompatibility and proliferation studies; mouse neuroblastoma cells (N2A) and immortalized human cortical neuronal cells (HCN1A), which are relevant for neurological applications and are characterized by low proliferation rates. Using silicon anodization, two classes of PSi substrates are fabricated within the MeP regime: MeP1 with a pore size of ∼5 nm and MeP2 with a pore size of ∼20 nm. After a through characterization of the silicon substrates, the distinctive cell adhesion behavior is documented using confocal and electron microscopy. The number density of adhering cells over the two PSi substrates and the flat unetched silicon, used as a control, is quantified at the different time points and compared across the different cells lines.

2. MATERIALS AND METHODS

2.1. Fabrication and Characterization of the PSi Substrates. A boron-doped, p type (100) silicon wafer (resistivity 5−10 Ω/cm) was used as a substrate. The silicon wafer was cleaned with acetone and ethanol to remove possible contaminants and then etched with a 4% wet HF (by Carlo Erba) solution. The wafer was rinsed with water and dried with N_2. PSi substrates with a pore diameter lower or equal to 10 nm were obtained by Si anodization using an electrolyte mixture of HF, D.I. water, and ethanol (by Sigma-Aldrich) (1:1:2, v/v/v). A constant current density of 20 mA/cm^2 for 5 min at 25 °C was applied. PSi substrates with a pore diameter larger than 10 and lower than 50 nm were obtained setting a constant current density of 4 mA/cm^2 for 5 min at 25 °C. An electrolyte mixture of HF, D.I. water, and methanol (by Sigma-Aldrich) (5:3:2, v/v/v) was used. The samples were finally rinsed in D.I. water, ethanol, and pentane with 4 min steps. The PSi substrates were finally oxidized in oven at 200 °C for 2 h.

The photoluminescence properties of the PSi substrate was directly verified using an ultraviolet lamp (from Spectroline), in the long wave ultraviolet limit (365 nm). The lamp was positioned at 25 cm from the sample, a distance that guarantees a typical peak intensity density of 1000 μm W/cm^2. The UV illumination was maintained for 10 s, and the samples were photographed with a commercial camera (Canon) setting 2 s integration time.

Surface hydrophilicity of the samples was determined by measuring the water contact angle with one drop of about 5 μL of D.I. water using an automatic contact angle meter (KSV CAM 101, KSV INSTRUMENTS LTD, Helsinki, Finland) at room temperature. Four measurements were performed on each substrate to evaluate the average contact angle θ, at 5 s.

2.2. Cell Culture and Staining. The four cell lines used, namely primary human endothelial (HUVEC-C), mouse mesenchymal normal (NIH-3T3), mouse neuroblastoma (Neuro-2a, N2A) and human cortical neuron cell line (HCN-1A) were obtained from the American Type Culture Collection (ATCC). The HUVECs were cultured in M199 medium containing 20% newborn calf serum (NCS, GIBCO-BRL), 5% human serum (Gemini Bio-Products, Inc.), 50 mg/mL ascorbic acid, 1.6 mmol/L L-glutamine, 5 mg/mL bovine brain extract (Clonetec Corp), 7.5 mg/mL endothelial growth supplement (Sigma), 100 U/mL penicillin, 100 mg/mL streptomycin, and 10 U/mL heparin. HUVECs at the third to fifth passage were used for all experiments. The 3T3, N2A and HCN-1A cells were cultured in Dulbecco's Modified Eagle's Medium (DMEM) with high glucose and GlutaMAXTM-I (Invitrogen, Carlsbad, California), supplemented with 10% fetal bovine serum (Invitrogen), penicillin G (100 U/ml) and streptomycin sulfate (100 mg/mL) (Invitrogen). PSi wafer specimens (15 × 15 mm approximately) were treated under UV light overnight for sterilization, then they were individually placed into single wells of a 6-well plate (Corning Incorporated). The wafer specimens were washed with phosphate-buffered saline solution (PBS, Invitrogen). The cells were finally seeded in complete cell culture medium and incubated for 24, 36, 48, and 60 h, at 37 °C in a humidified 5% CO_2/air atmosphere. After incubation, the cell culture medium was removed and the cells were washed twice in PBS and fixed with BD Cytofix (BD Biosciences). 100 μL of Cytofix were put on each sample and were incubated in dark for 30 min at 4 °C. The cells were washed twice with Cytoperm (a permeabilization solution, BD Biosciences). All cells fixed upon the Si substrates were labeled with 100 μL DAPI (40, 6-Diamidino-2-phenylindole, SigmaeAldrich) solution for 30 min at 4 °C. Finally, the DAPI solution was removed and each sample was washed with PBS. The total number of cells n_{tot} initially deposited in each well for incubation was 3.0×10^4, 1.5×10^4, 5.0×10^5, and 1.0×10^4 for the mouse 3T3 fibroblasts, the HUVECs, the N2A and the HCN-1A experiments, respectively. The cells were subconfluent throughout the duration of the experiment. Note that, although the number of originally seeded cells varies with the cell line, the area covered by the cells is smaller than about 1%, at time zero, and well below 80%, at 60 h post incubation. Therefore, the effect of the originally seeded number of cells on their viability and proliferation can be neglected.

Cells were washed twice in PBS and permeabilized with 0.5% Triton X-100 (SIGMA Aldrich, St. Louis, MO) for 15 min at room temperature. Then, cells were washed again twice in PBS, labeled with Vinculin primary antibody (Abcam) for 30 min at 4 °C and a secondary antibody (Alexa Fluor 488 chicken antimouse from Invitrogen) was added. After 40 min of incubation, the cells were washed twice with PBS and incubated with Alexa Fluor 635 phalloidin (Invitrogen). The samples were washed twice with PBS. After this, cells were labeled with 100 μL of DAPI solution (Sigma Aldrich) 30 min at 4 °C. And finally, each sample was washed three times with PBS.

2.3. Cell Microscopy and Counting. An inverted Leica TCS-SP2 laser scanning confocal microscopy system was used to image cells

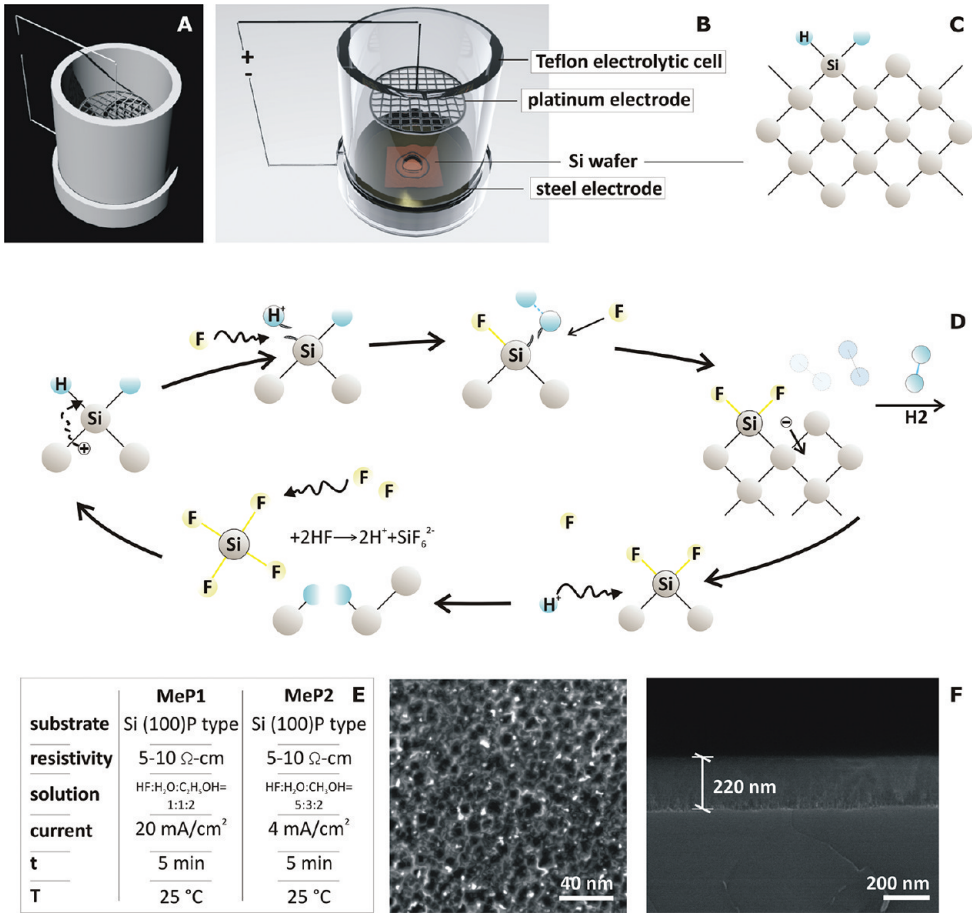

	MeP1	MeP2
substrate	Si (100)P type	Si (100)P type
resistivity	5-10 Ω-cm	5-10 Ω-cm
solution	HF:H_2O:C_2H_5OH= 1:1:2	HF:H_2O:CH_3OH= 5:3:2
current	20 mA/cm^2	4 mA/cm^2
t	5 min	5 min
T	25 °C	25 °C

Figure 1. Fabrication of porous silicon (PSi) substrates. (A, B) Images of the Teflon electrolytic cell used for the anodization of the silicon wafers. (C, D) Schematic of the reaction between silicon and the HF electrolytic solution, governing the porosification process. (E) Parameters used during the etching process for the different Psi substrates (MeP1 and MeP2). (F) Top view and later cross section of a porosified silicon surface substrate (MeP2).

adhering on the substrates. Confocal images of blue (DAPI) fluorescence were collected using a 405 nm excitation line and a 10× dry objective, so that cells with a characteristic size of a few micrometers could be clearly observed. The number of cells adhering to the substrate within the region of interest at different roughness and time steps was measured. The cells were analyzed over time after 24, 36, 48, and 60 h in culture. The number of adhering cells (n) was normalized with respect to the total number of cells initially deposited in each well (n_{tot}) and divided by the well area to derive the surface density of adhering cells as $n_d = n/(n_{tot}A)$ with $A \approx 707$ mm^2.

The fluorescence distribution of actin and vinculin was analyzed for cells deposited on flat and PSi substrates using an inverted Nikon TE2000-C1 confocal microscope. All images were acquired using a 60 × /1.49 NA TIRF oil immersion objective. The pinhole (30 μm) was maintained throughout each experiment, thus yielding the maximum confocality for the system. Sample fluorophores were excited using a 488 nm Ar Laser (for vinculin) and a 543 nm HeNe laser (for actin). The images were digitized into 512 × 512 pixels and conveyed to a computer for storage.

2.4. SEM Characterization of the PSi Substrates and Cells. SEM images of the wafers were captured using a Dual Beam (SEM-FIB) - FEI Nova 600 NanoLab system. During acquisition, the beam energy and the corresponding electron current were fixed to 15 keV and 0.14 nA, respectively. The PSi morphology was imaged by employing the mode 2 configuration, whereby images can be magnified over 2500 × 10^3 times and ultrahigh resolution can be achieved.

For cell characterization, the Si specimens were positioned inside each well in a 6 well micro plate. The cells were cultured for 48 h using normal conditions, as described above. The medium was removed by suction. The cells were then washed twice with PBS buffer and fixed with 4% of paraphormaldehyde for 30 min at 4 °C. The samples were washed twice with 0,1 M Cacodylate Buffer with 10 min wait between each washing. The sample were finally dehydrated using alcohol steps 10 min long, with a concentration in D.I. water ranging from 50 to 100% in volume. Several SEM images of the cells were captured to assess the dependence of cells morphology upon the different porous substrate. A JEOL JSM-7500F scanning electron microscope was used for the measurements. During acquisition, the beam energy of 5 keV and corresponding electron current of 0.98 pA was used.

The surface porosity of the substrates was determined by proper imaging analysis of several SEM micrographs, as described in the Supporting Information.

2.5. Cell Protein Extracts and Western Blot. The expression of vinculin, a major component of adhesion plaques and cell−cell junctions, is markedly up regulated in cells during growth activation, differentiation, motility and cell transformation. Therefore, experiments were performed to verify the expression of vinculin in cells growing on flat and MeP Si substrates. Neuro2a neuroblastoma cells were seeded on the different substrates and, after 48 h, the total protein was collected and subjected to Western blotting assay. Total protein extracts were obtained as follow: a 5 × 10^5 cell pellet was resuspended in 50 μL of RIPA buffer (50 mM Tris-cl pH 7.4; 150 mM NaCl; 1% NP40; 0.25% Na-deoxycholate; 1 mM PMSF; 1x Roche complete mini protease inhibitor cocktail; 1x Sigma phosphatase inhibitor 1 cocktail) and maintained for 20 min on ice with constant rocking. Samples were centrifuged 20 min at 12,000 rpm 4 °C and supernatant was collected in new tubes. Proteins were quantified by

dx.doi.org/10.1021/am300519a | ACS Appl. Mater. Interfaces 2012, 4, 2903−2911

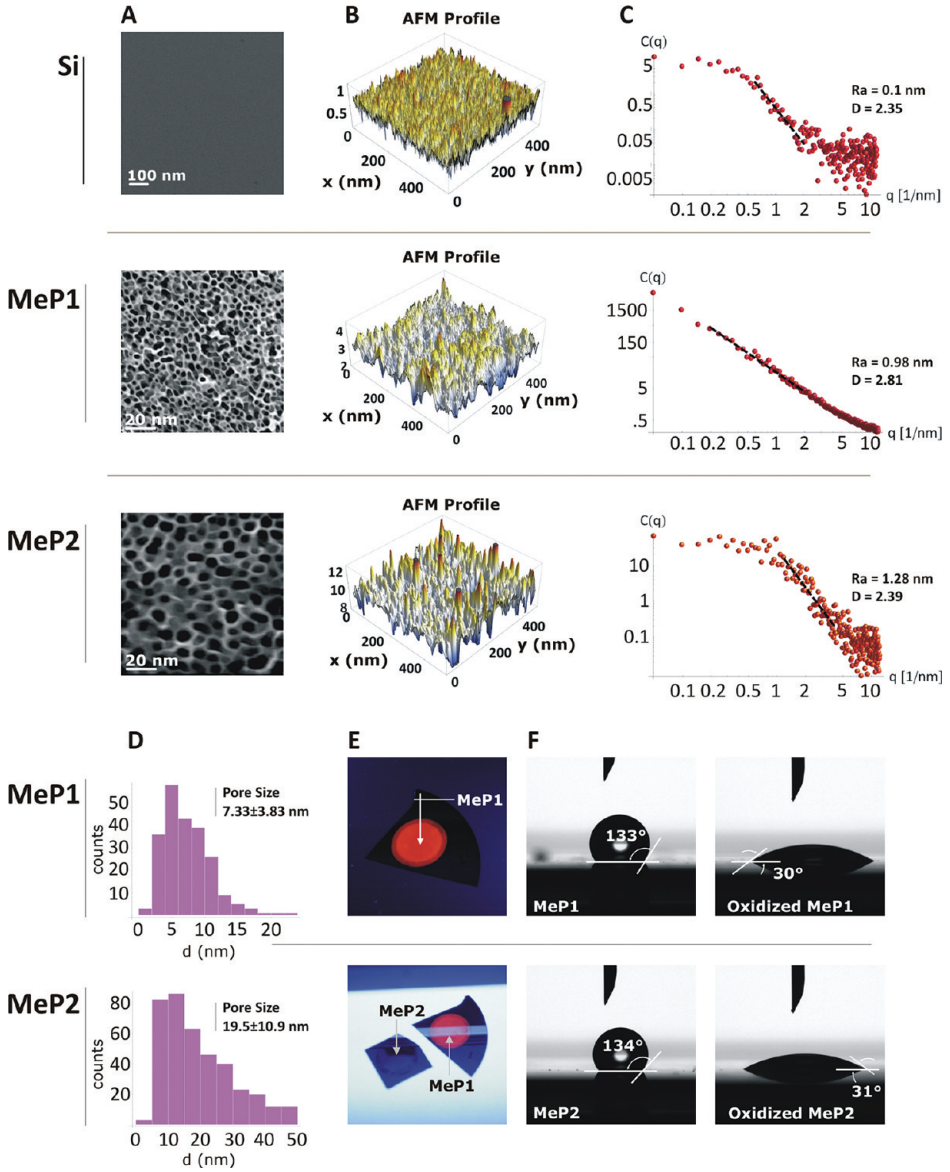

Figure 2. Characterization of the porous silicon (PSi) substrates. Surface topography of the silicon substrates imaged with (A) scanning electron microscopy and (B) atomic force microscopy. (C) Power spectrum of the silicon surfaces with the values for surface roughness R_a and fractal dimension D. (D) Pore size distribution for the porous silicon substrates, with the mean pore size. (E) Photoluminescence analysis for the two porous substrates. (F) Contact angle measurements for the two porous substrates before (left) and after (right) oxidation.

Lowry method (Bio-Rad Laboratories Inc., Hercules, CA, USA). Twenty μg of protein were subjected to Western blot in 10% SDS-PAGE. Antibodies were antivinculin (Abcam, Cambridge, UK), anti-β III tubulin (Santa Cruz Biotechnologies, Santa Cruz, CA, USA).

2.6. Statistical Analysis. Results are presented as mean ± SD. A student t test was used to compare two groups, fixing statistical significance at $p < 0.05$. p values smaller than 0.05 between two groups imply no statistically significant difference.

3. RESULTS

3.1. Fabrication and Characterization of Porous Silicon (PSi) Substrates. PSi substrates were generated from a bulk boron-doped p-type (100) silicon wafer via anodization.[1] The original silicon wafer was placed in a Teflon electrolytic cell, where a platinum cathode and the silicon wafer (anode) are immersed in a hydrogen fluoride (HF) solution (Figure 1A–C). The mechanism for pore formation is schematically reported in Figure.1D. Substrates with various pore sizes were obtained by tailoring the etching conditions (Table in Figure.1E), and treating the silicon wafers for 5 min at room temperature (25 °C). Mesoporous silicon substrates with an average pore diameter of 5 nm (MeP1) and 20 nm (MeP2) were obtained by applying a constant current density of 20 mA/cm^2 and 4 mA/cm^2, respectively. This anodization process introduced a thin porous layer over the original flat Si substrate with a thickness of a few tens of nanometers (Figure 1F). In this work, three substrates are used for the analysis of cell behavior: MeP1, MeP2 and flat unetched silicon (Si), as a reference.

The surface topography of the three substrates was analyzed using scanning electron microscopy (SEM) and atomic force microscopy (AFM). Also, photoluminescence was used to confirm indirectly the characteristic pore size in the MeP substrates; and contact angle measurements were employed to quantify the substrate hydrophobicity. Figure 2A–C shows representative SEM and AFM images of the three substrates,

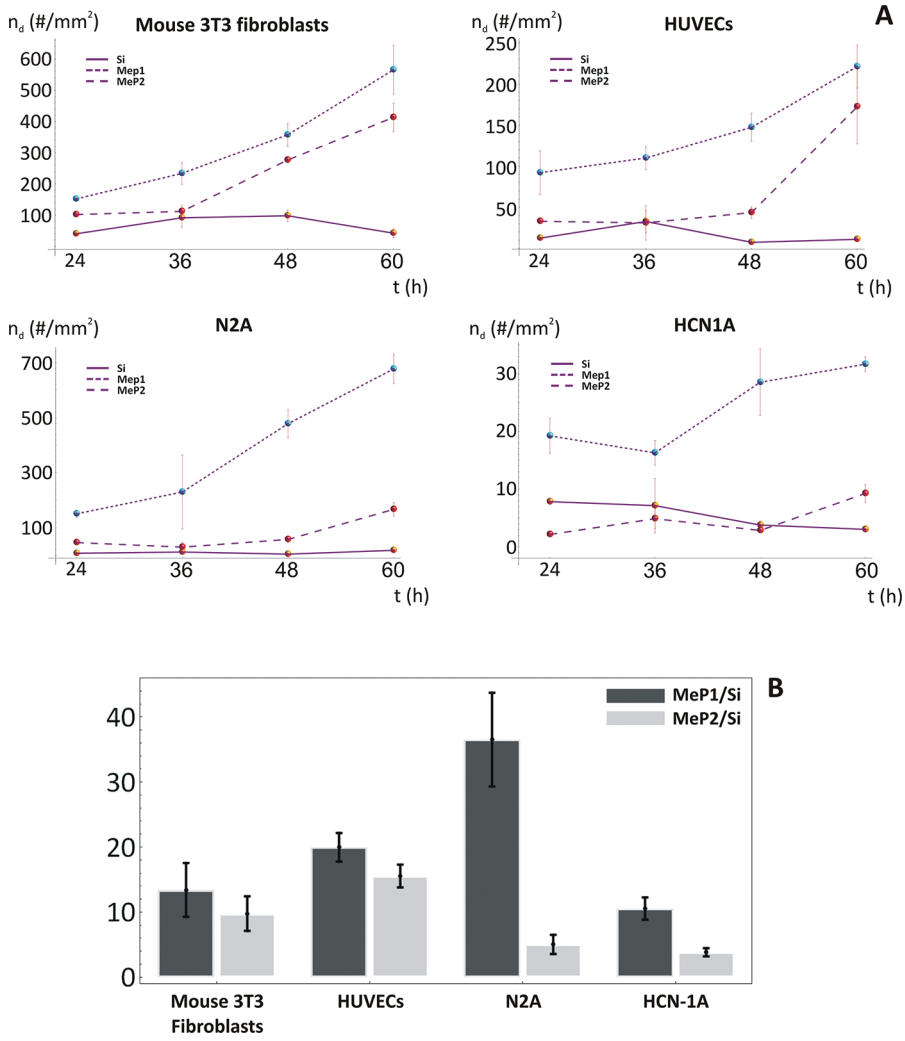

Figure 3. Cell proliferation on porous silicon (PSi) substrates. (A) Surface density nd for the four cells types (mouse 3T3 fibroblasts; HUVECs; N2A and HCN1A) as a function of the incubation time. Flat silicon (Si; blue line), mesoporous silicon MeP1 (pore size ∼5 nm; green line) and mesoporous silicon MeP2 (pores size ∼20 nm; red line). Four time points are considered: 24 h, 36 h, 48 h and 60 h post deposition. (B) Ratio between the surface density of cells growing on MeP1 and Si substrates (MeP1/Si) and on MeP2 and Si substrates (MeP2/Si), at 60 h post deposition.

together with a power spectrum analysis of the surface profile. Distinctive geometrical features can be easily depicted when comparing the three substrates (Figure 2A): the Si substrate appears as almost uniformly flat; the MeP1 and MeP2 substrates are quite uniformly porosified with a characteristic pore size in the few nanometers and few tens of nanometers, respectively. Such differences are also reflected by the surface AFM profiles (Figure.2B) and by the surface power spectra (Figure 2C). In particular, the surface roughness R_a is low for all three substrates being equal to 0.1, ∼1, and ∼1.3 nm for the Si, MeP1, and MeP2 substrates, respectively. On the other hand, larger differences arise for the surface fractal dimension D, when comparing Si and MeP2 (D = 2.35 and 2.39, respectively) with the MeP1 substrate (D = 2.81).

A detailed analysis of the pore geometry is presented in Figure 2D where the pore size distribution, photoluminescent behavior and surface contact angle are presented for the two PSi substrates. For MeP1 substrates, most of the pores have a size falling in the 5 nm range and no pores larger than 20 nm are detected; whereas for the MeP2 substrates, most of the pores exhibit a characteristic size ranging between 10 and 20 nm and very few pores are larger than 50 nm (Figure 2D). These pore size distributions are confirmed by the photoluminescence analysis where the silicon substrates are exposed to a UV light ($\lambda \approx 365$). As expected,[35] the images show a stronger luminescence for the MeP1 as compared to the MeP2 substrates, in that the former have a higher occurrence of pores in the nanometer range (Figure.2E). Both MeP substrates are originally hydrophobic exhibiting a contact angle of $\theta \approx 135°$, but becomes hydrophilic ($\theta \sim 30°$) upon oxidation (Figure.2F). The flat Si substrates are hydrophilic with a contact angle θ = 60° (see Figure S1 in the Supporting Information). By imaging postprocessing of several SEM micrographs, the surface porosity of the two Si substrates was estimated as the ratio between total area of the pores and the area of the considered region of interest. As shown in the Supporting Information, the surface porosities were 20.1 ± 4% for MeP1 and 25.0 ± 6% for MeP2.

3.2. Cell Adhesion and Proliferation on Porous Silicon (PSi) Substrates. The propensity to adhere and grow of the four cell types was analyzed by incubating them over fragments of silicon substrates (∼15 × 15 mm). Note that none of the

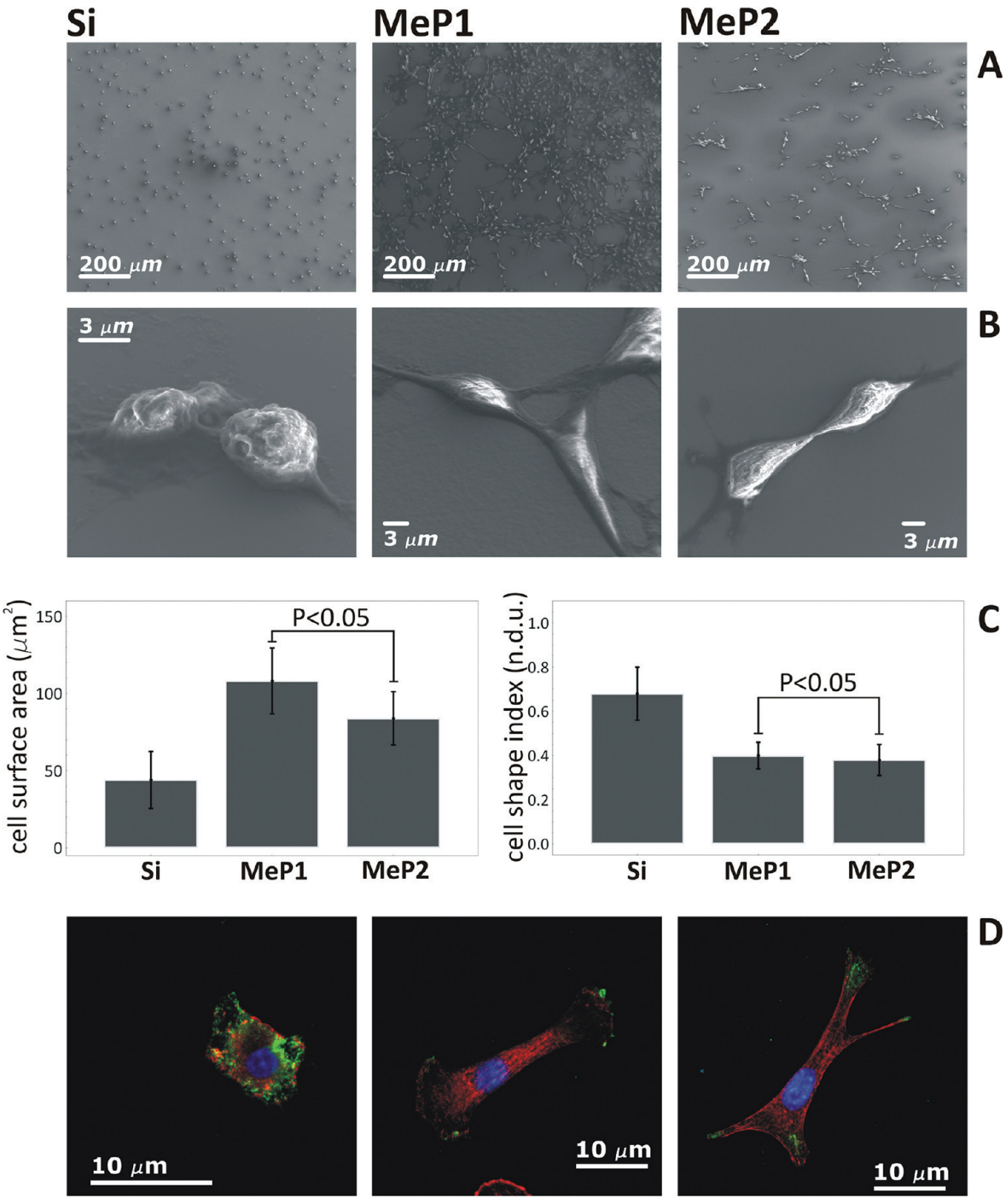

Figure 4. Cell morphological analysis of mouse 3T3 fibroblasts at 48 h. (A, B) Scanning electron micrographs of 3T3 cells growing on the three silicon substrates, at two magnifications. (C) Quantification of the cell covered area and cell shape factors over the three silicon substrates. (D) Confocal imaging for the cells stained for vinculin molecules (green), actin filaments (red), and nucleus (blue).

substrates was pretreated to support cell adhesion. At each time point, namely 24, 36, 48, and 60 h, the silicon substrates were first washed to remove loosely adhering and death cells; then, the remaining cells were fixed and labeled with DAPI. The cells adhering within a region of interest (ROI) of ~1 × 1 mm^2 were counted using fluorescent microscopy. For each substrate, more than 40 ROIs were considered to provide a meaningful sample size for statistical analysis

The number of adhering cells per unit surface normalized by the total number of seeded cells (i.e., the cell surface density, n_d) is shown in Figure 3A as a function of time. As expected, the cell surface density n_d increases with time. More interestingly, Figure 3A shows that the maximum cell surface density n_d occurs over the MeP1 substrates, at all time points and for all cell types. The contribution of the MeP1 substrates in supporting cell adhesion and proliferation is even more evident in the bar chart of Figure 3B, where the ratios between the cell surface densities n_d, measured at 60 h, over the MeP1 and Si substrates (MeP1/Si) and the MeP2 and Si substrates (MeP2/Si) are presented. For the first ratio, MeP1/Si substrate (dark bars in Figure 3B), values larger than 50 are observed for the neuronal N2A cells. These are followed by the mouse 3T3

fibroblasts, with a ratio larger than 10; HUVECs, with a ratio of ~7; and by the HCN-1A cells, with a ratio of ~5. The MeP2/Si ratios are smaller but still significantly larger than unity (light bars in Figure.3B). Comparing directly the surface density of cells on the two PSi substrates, it appears that cells are from ~1.5 to 5 times more numerous on MeP1, at 60 h. It is here important to recall that human cortical neuronal cells (HCN-1A) proliferate very slowly but, interestingly, they do exhibit a growth rate significantly larger than zero on MeP1 substrates. This experimental evidence supports the notion that cells preferentially adhere and grow over substrates with nanometer pore size (MeP1) rather than on flat Si substrates or substrates with a larger pore size (MeP2).

A direct comparison of the adhesion of 3T3 mouse fibroblasts and HUVECs on nominally flat silicon substrate (Si) and glass cell culture dish (Glass) has been included in Figure S2 in the Supporting Information. The data show minor differences in terms of the number density of cells adhering over 4 different times points, namely 24, 36, 48, and 60 h. The surface of the two substrates (Si and Glass) has also been characterized using Atomic Force Microscopy and Contact Angle measurements (see Figure S3 in the Supporting Information). These data show that the considered cell lines have fairly similar behaviors on Si and Glass, thus suggesting that the difference observed with the porous substrates is significant and practically relevant.

To gain additional information on the distinctive cell behavior over the three different substrates, the 3T3 and N2A cells were fixed and observed with scanning electron and confocal microscopy. SEM and fluorescent confocal microscopy images for the mouse 3T3 fibroblast cells are given in Figure 4. Similar images for the N2A cells are presented in Figure S4 in the Supporting Information. On both MeP substrates, the cell body appears elongated with a well spread cytoskeleton and the formation of long protrusions out of the cell membrane (Figure 4B, D). Differently, on the Si substrate, cells appear more rounded with a few short and squat protrusions (Figure 4B). Noticeably, and in accordance with these findings, a similar behavior was observed for stromal cells that, when adhering on mesoporous silicon or polymer fiber composites, exhibit elongated morphologies.[36] From the SEM images, two important parameters for characterizing the cell morphology can be derived: the cell area A (in μm^2), defined as the area covered by the cell projected over the substrate; the cell shape index (CSI), defined as the ratio between the shorter and the longer axis of the cell. Both parameters, A and CSI, are presented in the bar chart of Figure 4C. For both MeP substrates, no significant difference is observed in cell adhesion area and morphology, whereas cells on flat Si substrates are more rounded and less spread. Note that flat Si substrates showed a slightly larger contact angle as compared to the MeP substrates, which could in part be responsible for the observed lower cell adhesion and spreading.

Similar morphological observations can be drawn from the confocal fluorescent images of Figure 4D. Here, however, additional information can be gained by looking at the actin network (red labeled) and the pattern distribution of the vinculin molecules (green labeled). Actin filaments appear more elongated and aligned along the major axis of the cell on the MeP substrates. Also, vinculin tends to form more distinct and ordered clusters, preferentially expressed at the head of cell membrane protrusions (Figure.4D). The higher expression levels of vinculin in cells growing on MeP substrates are also confirmed by Western blotting analysis: as shown in Figure S5 in the Supporitng Information, the signal given by antivinculin antibody appeared 2 times higher in Neuro2A proliferating on MeP1 substrate, compared to Si and MeP2. No difference was revealed in beta-III tubulin expression, used as calibrator. Taken together, these results indicate that cells growing on MeP1 substrates can better activate molecular pathways directly related to the active proliferation.

It should here be noted that in a biological environment (pH > 5.5), porous silicon is generally biodegradable over time.[43−46] The dissolution process is strongly dependent on the porosity of the layer and surface modification. The substrates used here exhibit a porosity not exceeding 60% and a protective coating of native silicon dioxide layer (SiO_2); and no substrate degradation was observed over the whole period of the experiments (60 h).

4. DISCUSSION

PSi implants for long-term drug release have been demonstrated for quite a few applications. This includes devices for the release of antibiotics in bone implants,[20,37,38] for supporting the differentiation and proliferation of stem cells,[23] hepatocites,[22] and improving the biomechanical connectivity between man-made electrodes and neuronal cells.[21] Drugs and small molecules can be effectively loaded into the porous network of PSi, using different approaches.[39,40] Capillary action is certainly the simplest. In this case, a concentrated solution of the active agent to be loaded is either dropped directly on the PSi layer or the latter is fully immersed in the solution. The pore geometry, as well as the surface chemical modification, are important determinants in controlling the loading, first, and then the release of the active agent.[41,42] Drugs, microbicidal formulations, proteins and small molecules are more effectively trapped in pores exhibiting a size smaller than ~10 nm. Indeed, this manuscript focuses on the behavior of cells that would adhere and proliferate over MeP1 (pore diameters <10 nm) and MeP2 (pore diameters = 10−50 nm) substrates.

The results presented clearly support the notion that cells can sense nanoscopic features on PSi substrates down to just a few nanometers (~ 5 nm) and react differently to distinctive nanotopographical cues. This has been demonstrated for four distinct cell types, namely mouse 3T3 fibroblasts, HUVECs, N2A and HCN-1A cells. They all manifested a higher adhesion on MeP1 substrates as compared to flat silicon or MeP2 surfaces, at all the considered time points. The largest enhancement in cell adhesion is observed for the N2A, a murine neuroblastoma cell line, for which 50 times more cells adhered, at 60 h, over the MeP1 substrates. But even the HCN-1A cells, which are characterized by a very slow proliferation rate, were observed to grow 5 times faster at 60 h. At authors' knowledge, such a behavior has never been reported, so far, since studies on cell adhesion over PSi have mostly focused on substrates with larger pores (>20−30 nm up to a few micrometers), showing either a decrease in adhesion (substrates with 100−500 nm pore size) or similar adhesion (>1000 nm), with respect to flat silicon wafers.[32−34]

It is still not yet clear, however, why cells would preferentially adhere and grow on MeP substrates. Recently, it has been shown that focal adhesions (FAs) exhibit a complex multiscale architecture where nanoscopic, doughnut-shaped complexes (~25 nm in diameter and spaced at ~45 nm intervals) are distributed within the adhesion area and are associated to aligned bundles of actin filaments.[47] Given their characteristic

size, these complexes could better conform to clusters of ~5 nm pores over MeP substrates. In other words, it can be speculated that the nanoscopic complexes in FAs would more intimately interact with the porous structure of the MeP substrates. More studies are needed to verify this hypothesis as well as to elucidate the role played by the nanoscopic complexes in FAs. In future works, the attention should focus on the systematic analysis of (i) the cytoskeleton organization via fluorescent confocal microscopy, (ii) the architecture of FAs by cryo-electron tomography; and (iii) the dynamics of formation for FXs and FAs. It should also be noted that an accurate dissection of the mechanisms regulating cell interaction with mesoporous structures would require the use of substrates that are transparent to light. Nonetheless, the MeP silicon substrates and the presented results help in shedding new lights on the biophysics of cell adhesion on truly nanoscopic substrates and stimulate additional work on this important subject.

5. CONCLUSIONS

The adhesion of four cell types, mouse 3T3 fibroblasts, HUVECs, N2A and HCN-1A cells, were monitored up to 60 h on three different silicon substrates: two PSi substrates, with a pore size falling in the mesoporous regime (MeP1: pore size ~5 nm; MeP2: pore size ~20 nm), obtained via anodization of silicon wafers and a unetched Si substrate.

Cells on MeP1 were documented to grow from 5 to 50 times faster as compared to Si substrates, at 60 h. For the MeP2 substrates, the growth rate was still larger than for the Si substrate and ranged between 1.5 and 8, at 60 h. The growth rate was higher for the N2A, a murine neuroblastoma cell line, and smaller for the HCN-1A, a human neuronal cell line which is known to have a very low duplication rate.

A large difference in adhesion between MeP1 and MeP2 was observed, although cell spreading and morphology appeared similar. We speculate that there could be an "optimal matching" between the multiscale molecular architecture of focal adhesions and the porous structure of MeP1 substrates that could facilitate adhesion.

These results have implications in the rational development of PSi substrates in implants and scaffolds for the controlled release of drugs, nerve repair, and tissue engineering applications.

■ ASSOCIATED CONTENT

Supporting Information

Additional data on the characterization of the PSi substrates and on cell adhesion, and complementary information to the Materials and Methods section. This material is available free of charge via the Internet at http://pubs.acs.org/.

■ AUTHOR INFORMATION

Corresponding Author

*E-mail pdecuzzi@tmhs.org. Phone: +1 713 441 7316.

Notes

The authors declare no competing financial interest.

■ ACKNOWLEDGMENTS

This research activity has been supported by the European Science Foundation EUROCORES Programme FANAS, through funds by the Consiglio Nazionale delle Ricerche and the EC Sixth Framework Programme under Contract ERAS-CT-2003-980409FANAS, and by the EU Commission, the European Social Fund and the Calabria Region (POR Calabria FSE 2007-2013).

■ REFERENCES

(1) Foll, H.; Christophersen, M.; Carstensen, J.; Hasse, G. *Mater. Sci. Eng.* **2002**, *39*, 93−141.
(2) Salonen, J.; Lehto, V. P. *Chem. Eng. J.* **2008**, *137*, 162−172.
(3) Buriak, J. M. *Chem. Rev.* **2002**, *102*, 1271−1308.
(4) Anderson, S. H. C.; Elliott, H.; Wallis, D. J.; Canham, L. T.; Powell, J. J. *Phys. Status Solidi* **2003**, *197*, 331−335.
(5) Canham, L. T.; Stewart, M. P.; Buriak, J. M.; Reeves, C. L.; Anderson., M.; Squire, E. K.; Allcock, P.; Snow, P. A. *Phys. Status Solidi A.* **2000**, *182*, 521−525.
(6) Bayliss, S. C.; Heald, R.; Fletcher, D. I.; Buckberry, L. D. *Adv. Mater.* **1999**, *11*, 318−321.
(7) Ainslie, K. M.; Tao, S. L.; Popat, K. C.; Desai, T. A. *ACS Nano* **2008**, *2*, 1076−1084.
(8) Lin, V. S. Y.; Motesharei, K.; Dancil, K. P. S.; Sailor, M. J.; Ghadiri, M. R. *Science* **1997**, *278*, 840−843.
(9) Canham, L. T. *Appl. Phys. Lett.* **1990**, *57*, 1046−1048.
(10) Cullis, A. G.; Canham, L. T.; Calcott, P. D. J. *J. App. Phys.* **1997**, *82*, 909−966.
(11) Desai, T. A.; Hansford, D. J.; Kulinsky, L.; Nashat, A. H.; Rasi, G.; Tu, J.; Wang, Y.; Zhang, M.; Ferrari, M. *Biomed. Microdevices* **1999**, *2*, 11−40.
(12) Anglin, E. J.; Cheng, L.; Freeman, W. R.; Sailor, M. J. *Adv. Drug Delivery Rev.* **2008**, *60*, 1266−1277.
(13) Perelman, L. A.; Pacholski, C.; Li, Y. Y.; Van Nieuwenhze, M. S.; Sailor, M. J. *Nanomedicine* **2008**, *3*, 31−43.
(14) Park, J. H.; Gu, L.; von Maltzahn, G.; Ruoslahti, E.; Bhatia, S. N.; Sailor, M. J. *Nat. Mater.* **2009**, *8*, 331−336.
(15) Tanaka, T.; Mangala, L. S.; Vivas-Mejia, P. E.; Nieves-Alicea, R.; Mann, A. P.; Mora, E.; Han, H. D.; Shahzad, M. M. K.; Liu, X.; Bhavane, R.; Gu, J.; Fakhoury, J. R.; Chiappini, C.; Lu, C.; Matsuo, K.; Godin, B.; Stone, R. L.; Nick, A. M.; Berestein, G. L.; Sood, A. K.; Ferrari, M. *Cancer Res.* **2010**, *70*, 3687−96.
(16) Ananta, J. S.; Godin, B.; Sethi, R.; Moriggi, L.; Liu, X.; Serda, R. E.; Krishnamurthy, R.; Muthupillai, R.; Bolskar, R. D.; Helm, L.; Ferrari, M.; Wilson, L. J.; Decuzzi, P. *Nat. Nanotechnol.* **2010**, *5*, 815−821.
(17) Jane, A.; Dronov, R.; Hodges, A. *Trends Biotechnol.* **2009**, *27*, 230−239.
(18) Hu, Y.; Bouamrani, A.; Tasciotti, E.; Li, L.; Liu, X.; Ferrari, M. *ACS Nano* **2010**, *4*, 439−451.
(19) Chan, S.; Fauchet, P. M.; Li, Y.; Rothberg, L. J.; Miller, B. L. *Phys. Status Solidi A* **2000**, *182*, 541−546.
(20) Wang, M.; Coffer, J. L.; Dorraj, K.; Hartman, P. S.; Loni, A.; Canham, L. T. *Mol. Pharm.* **2010**, *7*, 2232−42.
(21) Moxon, K. A.; Hallman, S.; Aslani, A.; Kalkhoran, N. M.; Lelkes, P. I. *J. Biomater. Sci., Polym. Ed.* **2007**, *18*, 1263−1281.
(22) Chin, V.; Collins, B. E.; Sailor, M. J.; Bhatia, S. N. *Adv. Mater.* **2001**, *13*, 1877−1880.
(23) Low, S. P.; Voelcker, N. H.; Canham, L. T.; Williams, K. A. *Biomaterials* **2009**, *30*, 2873−80.
(24) Curtis, A.; Wilkinson, C. *Biomaterials* **1997**, *18*, 1573−1583.
(25) Dalby, M. J.; Riehle, M. O.; Yarwood, S. J.; Wilkinson, C. D. W.; Curtis, A. S. G. *Exp. Cell. Res.* **2003**, *284*, 274−282.
(26) Andersson, A. S.; Backhed, F.; von Euler, A.; Richter-Dahlfors, A.; Sutherland, D.; Kasemo, B. *Biomaterials* **2003**, *24*, 3427−36.
(27) Choi, C. H.; Hagvall, S. H.; Wu, B. M.; Dunn, J. C. Y.; Beygui, R. E.; Kim, C. J. *Biomaterials* **2007**, *28*, 1672−79.
(28) Brunetti, V.; Maiorano, G.; Rizzello, L.; Sorce, B.; Sabella, S.; Cingolani, R.; Pompa, P. P. *Proc. Natl. Acad. Sci. U.S.A.* **2010**, *107*, 6264−9.
(29) Gentile, F.; Tirinato, L.; Battista, E.; Causa, F.; Liberale, C.; Di Fabrizio, E. M.; Decuzzi, P. *Biomaterials* **2010**, *31*, 7205−12.

(30) Low, S. P.; Williams, K. A.; Canham, L. T.; Voelcker, N. H. *Biomaterials* **2006**, *27*, 4538−46.
(31) Zhao, Y.; Lü., X.; Wang, Z.; Huang, Y.; Jiang, Z.; Li, X. *Biomed. Mater.* **2009**, *4*, 065004−9.
(32) Sapelkin, A. V.; Bayliss, S. C.; Unal, B.; Charalambou, A. *Biomaterials* **2006**, *27*, 842−6.
(33) Khung, Y. L.; Barritt, G.; Voelcker, N. H. *Exp. Cell. Res.* **2008**, *314*, 789−800.
(34) Orita, T.; Tomita, M.; Kato, K. *Colloids Surf., B* **2011**, *84*, 187−97.
(35) Godefroo, S.; Hayne, M.; Jivanescu, M.; Stesmans, A.; Zacharias, M.; Lebedev, O. I.; Van Tendeloo, G.; Moshchalkov, V. V. *Nat. Nanotechol.* **2008**, *3*, 174−8.
(36) Fan, D.; Akkaraju, G. R.; Couch, E. F.; Canham, L. T.; Coffer, J. L. *Nanoscale* **2011**, *3*, 354−61.
(37) Perez, L. M.; Lalueza, P.; Monzon, M.; Puertolas, J. A.; Arruebo, M.; Santamaría, J. *Int. J. Pharm.* **2011**, *409*, 1−8.
(38) Gultepe, E.; Nagesha, D.; Sridhar, S.; Amiji, M. *Adv. Drug Delivery Rev.* **2010**, *62*, 305−15.
(39) Anglin, E. J.; Cheng, L; Freeman, W. R.; Sailor, M. J. *Adv. Drug Delivery Rev.* **2008**, *60*, 1266−77.
(40) Salonen, J.; Kaukonen, A. M.; Hirvonen, J.; Lehto, V. P. *J. Pharm. Sci.* **2008**, *97*, 632−53.
(41) Leoni, L.; Boiarski, A.; Desai, T. A. *Biomed. Microdev.* **2002**, *4*, 131−139.
(42) Tasciotti, E.; Liu, X.; Bhavane, R.; Plant, K.; Leonard, A. D.; Price, B. K.; Cheng Cheng, M. M.; Decuzzi, P.; Tour, J. M.; Robertson, F.; Ferrari, M. *Nat. Nanotechnol.* **2008**, *3*, 151−157.
(43) Canham, L. T. *Adv. Mater.* **1995**, *7*, 1033−37.
(44) Canham, L. T.; Reeves, C. L.; Newey, J. P.; Houlton, M. R.; Cox, T. I.; Buriak, J. M.; Stewart, M. P. *Adv. Mater.* **1999**, *11*, 1505−07.
(45) Steinem, C.; Janshoff, A.; Lin, V. S. Y.; Völcker, N. H.; Ghadiri, M. R. *Tetrahedron* **2004**, *60*, 11259−11267.
(46) Canham, L. T. *Properties of Porous Silicon*; Institute of Engineering and Technology: Stevenage, U.K., 1997.
(47) Patla, I.; Volberg, T.; Elad, N.; Hirschfeld-Warneken, V.; Grashoff, C.; Fässler, R.; Spatz, J. P.; Geiger, B.; Medalia, O. *Nat. Cell Biol.* **2010**, *12*, 909−15.